

# Synthesis and structural Characterization of Cu Substituted SrCoO<sub>3-δ</sub> Perovskite Oxides

Lynda Djoudi<sup>1,\*</sup>, Belkis Bourmal<sup>2</sup> and Mahmoud Omari<sup>1</sup>

<sup>1</sup>Laboratory of Molecular Chemistry and Environment, University Mohamed Khider of Biskra, 07000 - Algeria

<sup>2</sup> Department of Science Material, chemistry, Faculty of Exact and Natural Sciences, University Mohamed Khider of Biskra, 07000 – Algeria

\* Corresponding author, e-mail address: [lynda.djoudi@univ-biskra.dz](mailto:lynda.djoudi@univ-biskra.dz)

Received 26 July 2022; accepted 16 November 2022; published online 20 December 2022

## ABSTRACT

In this work, SrCo<sub>1-x</sub>Cu<sub>x</sub>O<sub>3-δ</sub> perovskite-type metal oxides (x = 0.00, 0.1, 0.2, 0.3) were prepared by sol-gel method using citric acid as chelating agent. We have focused on examining the effect of partial substitution of cobalt by copper on the phase purity and crystallinity of the end products. The samples obtained after calcination at 900°C for 6h were characterized by X-ray diffraction (XRD), Fourier transform infrared spectroscopy (IRTF) and powder size distribution (PSD).

XRD patterns indicate that a perovskite structure with rhombohedral system has been obtained for all the compositions with no detectable secondary phase where the crystallite size ranges from 48.74 to 53.49 nm. The crystallite size decreases with increasing the copper amount. The grain size of oxides as determined from laser diffraction ranges from 0.213 to 0.307 micron, this result reveals that agglomerates are present in the suspension. Infrared spectroscopy shows a broad characteristic band of absorption observed around 581 cm<sup>-1</sup> was attributed to the BO (Co-O, Cu-O) stretching vibration. This band is characteristic of the perovskite structure ABO<sub>3</sub>.

## 1. INTRODUCTION

Perovskite oxides, with a general formula of ABO<sub>3</sub>, have been a research hot spot due to their considerable reserves of raw metals and flexible adjustability [1-3]. It is an effective strategy to adjust the physicochemical properties of the perovskite by partial substitution of the A-site or B-site metals [4-7]. Depend on this compositional diversity and adjustable properties, perovskite oxides have been tried to be applied in a great many of fields, including solid oxide fuel cells, metal-air batteries, and oxygen permeation membranes [8-10].

Perovskite-type mixed ionic and electronic conducting (MIEC) materials have high flexibility to tune their physical properties such as oxygen vacancies, structural symmetry, lattice free volumes and metal-oxygen bonding energies.

These properties are strongly dependent on crystal structure and significantly affect electrochemical kinetic properties and stability of the materials [11, 12].

Strontium cobaltite (SrCoO<sub>3-δ</sub>) is a typical perovskite MIEC showing high electrical conductivity and electrocatalytic property as a cathode material for solid oxide fuel cell (SOFC) and has been widely used as a parent compound to derive other high performance MIEC cathodes [13]. Depending on annealing temperature and oxygen partial pressure during synthesis/fabrication process, SrCoO<sub>3-δ</sub> may adopt a variety of crystal structures, e.g., orthorhombic, tetragonal and cubic. For example, SrCoO<sub>3-δ</sub> forms an oxygen vacancy-ordered orthorhombic brownmillerite phase below 653 °C and will transfer to a 2-H type hexagonal phase between 653 and 920°C, eventually changes to a cubic or tetragonal

perovskite phase above 920 °C. However, the high temperature phase will transit reversibly to a hexagonal phase as temperature drops from a high (> 920°C) to intermediate temperature range [14].

In this work, SrCo<sub>1-x</sub>Cu<sub>x</sub>O<sub>3-δ</sub> perovskite-type metal oxides (x = 0.00, 0.1, 0.2, 0.3) were prepared by citrate sol-gel method. We have focused on examining the influence of copper concentration on the phase purity and crystallinity of the end products.

## 2. EXPERIMENTAL PROCEDURE

### 2.1. Powder Synthesis

All the solvents and chemicals were of analytical grade and used without any further purification. A sol-gel route with citric acid was adopted to synthesize SrCo<sub>1-x</sub>Cu<sub>x</sub>O<sub>3-δ</sub> nanoparticles with x = 0.00, 0.1, 0.2, and 0.3. An estimated quantity of Sr(NO<sub>3</sub>)<sub>2</sub>, Co(NO<sub>3</sub>)<sub>2</sub>·6H<sub>2</sub>O and C<sub>6</sub>H<sub>8</sub>O<sub>7</sub>, H<sub>2</sub>O were dissolved separately in distilled water with magnetic stirring for 15 min. Afterward, the mixture was vigorously stirred on a hot plate at 80 C° for 4 h. The viscous gel was further dried for 12 h at 110 C° in an oven and ground into powder. Subsequently the powder was calcined for 6 h in air at 900 C°. In a similar process, the SrCo<sub>1-x</sub>Cu<sub>x</sub>O<sub>3-δ</sub> nanoparticles were synthesized by following the above defined steps of sol-gel

method. The estimated amount of dopant copper nitrate was added in the precursor solution and other conditions of synthesis were kept unchanged.

### 2.2. Characterization

The eventual presence of organic material after calcination was determined by infrared spectroscopy within the interval from 4000 to 400 cm<sup>-1</sup> using FT-IR SHIMADZU 8400S spectrometer. The sample was mixed with dry KBr to form a pellet for the measurement. X-ray diffraction (XRD) patterns were carried out with a D8 ADVANCE-BRUCKER using a Cu Kα radiation (λ<sub>Kα</sub> = 1.54056 Å) and a Ni filter. The powder samples were mounted on a flat XRD plate and scanned at room temperature in the range 10°- 90° to identify the crystalline phases present in the calcined powders by comparison with Joint Committee on Powder Diffraction Standards (JCPDS) files. The crystallite size (D) was evaluated from the broadening of the X-ray diffraction peaks using Scherrer's formula. The average particle size distribution was determined using the laser diffraction method fitted with a wet sampling system (Malvern, Mastersizer 2000).

## 3. RESULTS AND DISCUSSION

### 3.1. Infrared Spectra

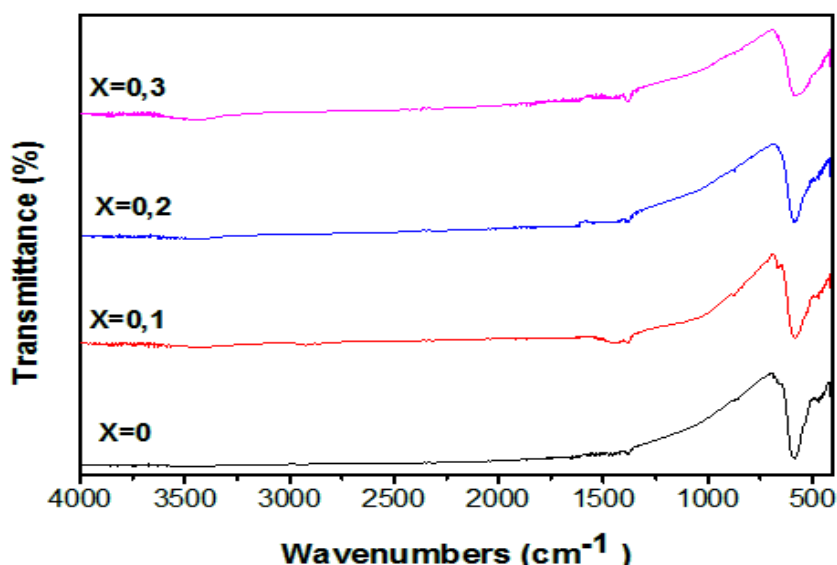


Figure 1. FT- IR absorption spectra of SrCo<sub>1-x</sub>Cu<sub>x</sub>O<sub>3-δ</sub> (x = 0.0-0.3).

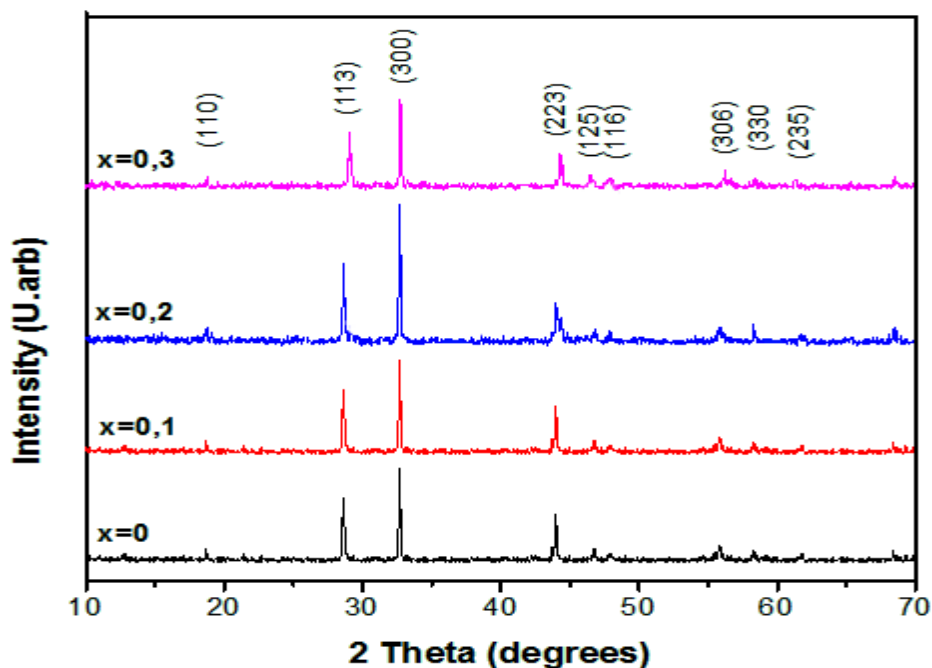


Figure 2. X-ray diffraction patterns of perovskite samples  $\text{SrCo}_{1-x}\text{Cu}_x\text{O}_{3-\delta}$  ( $x = 0.0-0.3$ ).

IR analysis of synthesized samples is important both for the control of the reaction process and the properties of materials obtained. The infrared spectra of the  $\text{SrCo}_{1-x}\text{Cu}_x\text{O}_{3-\delta}$  samples (Figure 1) are presented in the  $400-4000\text{ cm}^{-1}$  region of the IR spectrum. The higher frequency band around  $581\text{ cm}^{-1}$  was assigned to the B–O stretching vibration mode (possible Co–O or Cu–O stretching

frequencies vibrations). This band is characteristic of the perovskite structure  $\text{ABO}_3$  [15]. No specific peaks of inorganic residues were observed suggesting the high purity of the resulting powders. These results are in accordance with the XRD analysis (Figure 2) which confirmed the formation of only crystalline phase in  $\text{SrCo}_{1-x}\text{Cu}_x\text{O}_{3-\delta}$  nanopowders.

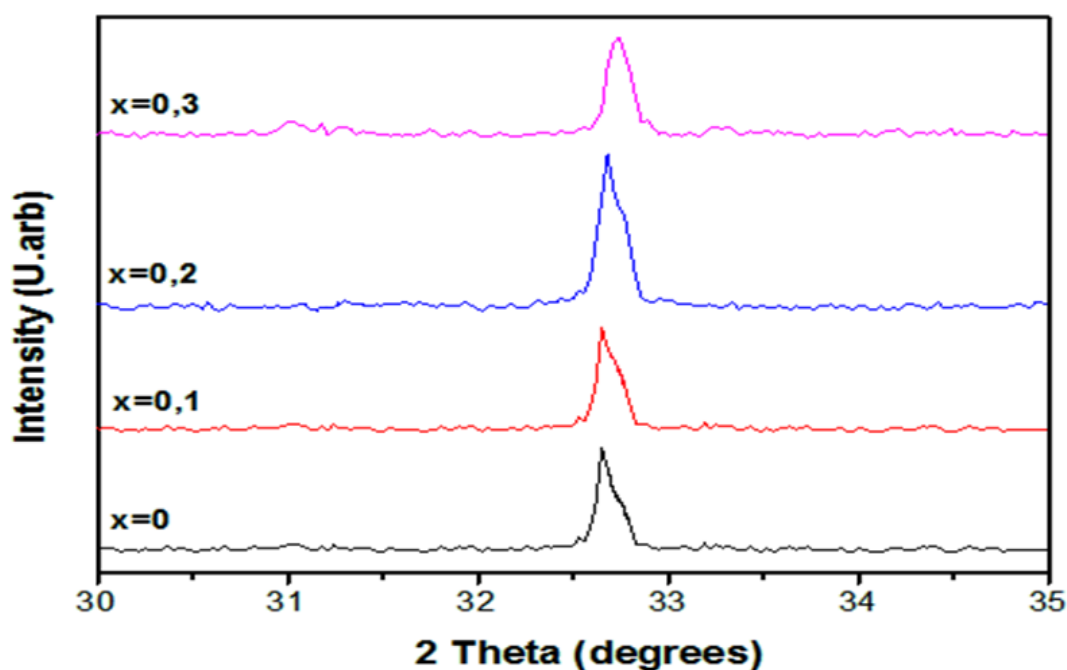


Figure 3. XRD patterns of  $\text{SrCo}_{1-x}\text{Cu}_x\text{O}_{3-\delta}$  with enlarged view around (300).

Table 1. Lattice parameters for  $\text{SrCo}_{1-x}\text{Cu}_x\text{O}_{3-\delta}$ .

Cu content x	a=b (Å)	c(Å)	V(Å <sup>3</sup> )
x=0	9.4890	12.3650	964.2
x=0.1	9.4845	12.3637	963.435
x=0.2	9.4797	12.3493	962.656
x=0.3	9.4788	12.3456	961.117

### 3.2. Structural characterization

The XRD patterns of the catalysts powders  $\text{SrCo}_{1-x}\text{Cu}_x\text{O}_{3-\delta}$  ( $x=0, 0.1, 0.2, 0.3$ ) obtained by citrate sol-gel method after calcinations at 900 °C for 6 h summarized in Figure 2, were compared to the relevant data in the Data Bank available in the diffractometer. We observed that all the diffraction peaks matched well with the rhombohedral structure of pure  $\text{SrCoO}_{3-\delta}$ . They are in excellent accord with JCPDS card 00-049-0692. The pattern clearly indicates the absence of any kind of impurity phases. This shows the proper incorporation and dispersion of  $\text{Cu}^{2+}$  ions into the  $\text{SrCoO}_{3-\delta}$  matrix.

The magnified view around  $2\theta$  30 and 35 was shown in Figure 3. With increase Cu concentration, XRD peak shifted slightly toward a higher  $2\theta$  angles (right shift), which demonstrated that the

$\text{Cu}^{2+}$  ion was successfully incorporated into the lattice of perovskite structure.

The lattice parameters of the perovskites  $\text{SrCo}_{1-x}\text{Cu}_x\text{O}_{3-\delta}$  were calculated for each x value from the XRD patterns using Celref programme. The values of a and c cell parameters (Å) versus the degree of substitution x are given in Table 1.

The values of the lattice parameters decrease with the increasing copper content in the samples from 0 to 0.3 (Table 1 and Figure 4). Such a decrease is also a confirmation for the Cu (II) substitution to Co (II) in the  $\text{SrCoO}_{3-\delta}$  crystal lattice. The substitution of  $\text{Co}^{2+}$  ions ( $r_{\text{Co}^{2+}} = 0.745$  Å) by smaller  $\text{Cu}^{2+}$  ions ( $r_{\text{Cu}^{2+}} = 0.73$  Å) [16] led to the reduction of the unit cell parameters. A similar observation was found in  $\text{SrCo}_{1-x}\text{Ni}_x\text{O}_{3-\delta}$  systems [17].

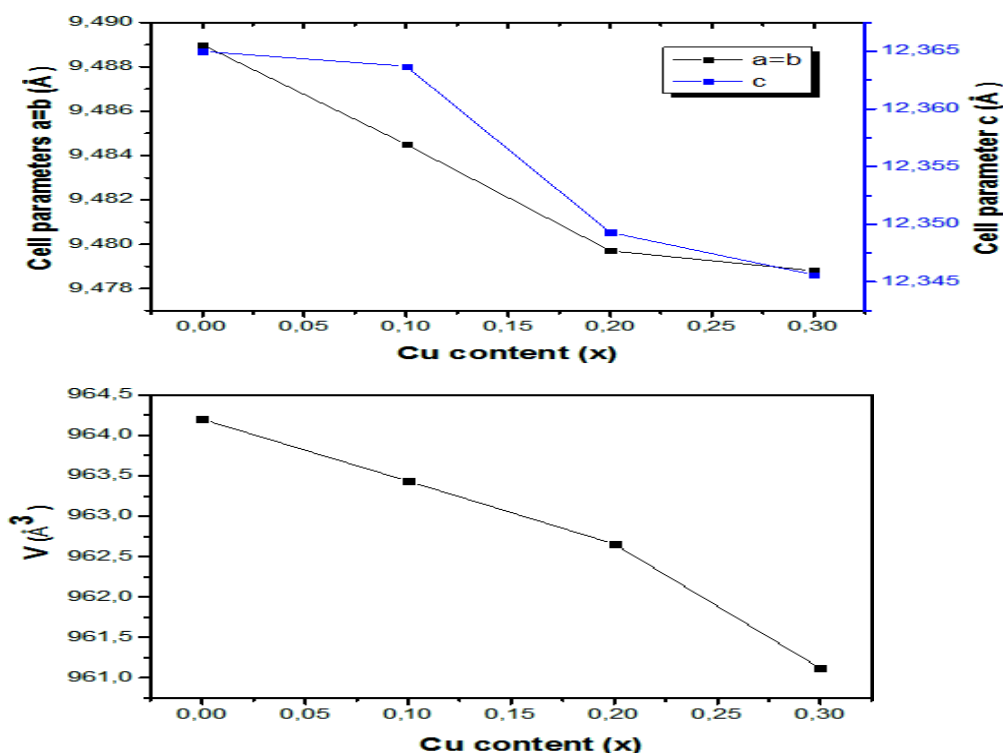


Figure 4. Evolution of lattice and volume parameters a function of copper content.

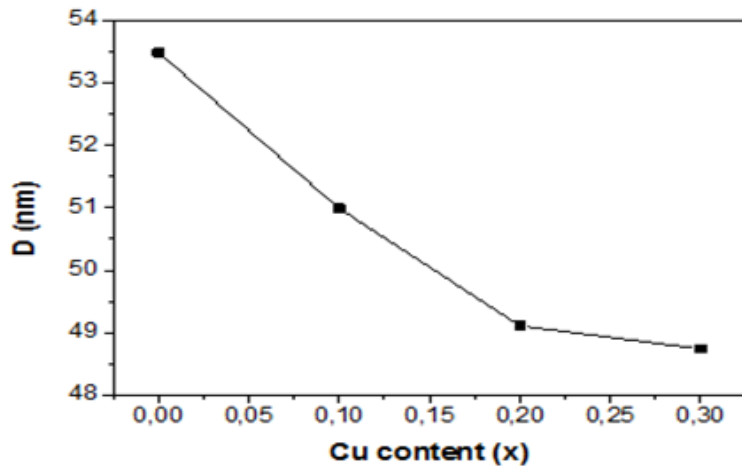


Figure 5. Crystallite size of SrCo<sub>1-x</sub>Cu<sub>x</sub>O<sub>3-δ</sub> powders (x = 0.0-0.3).

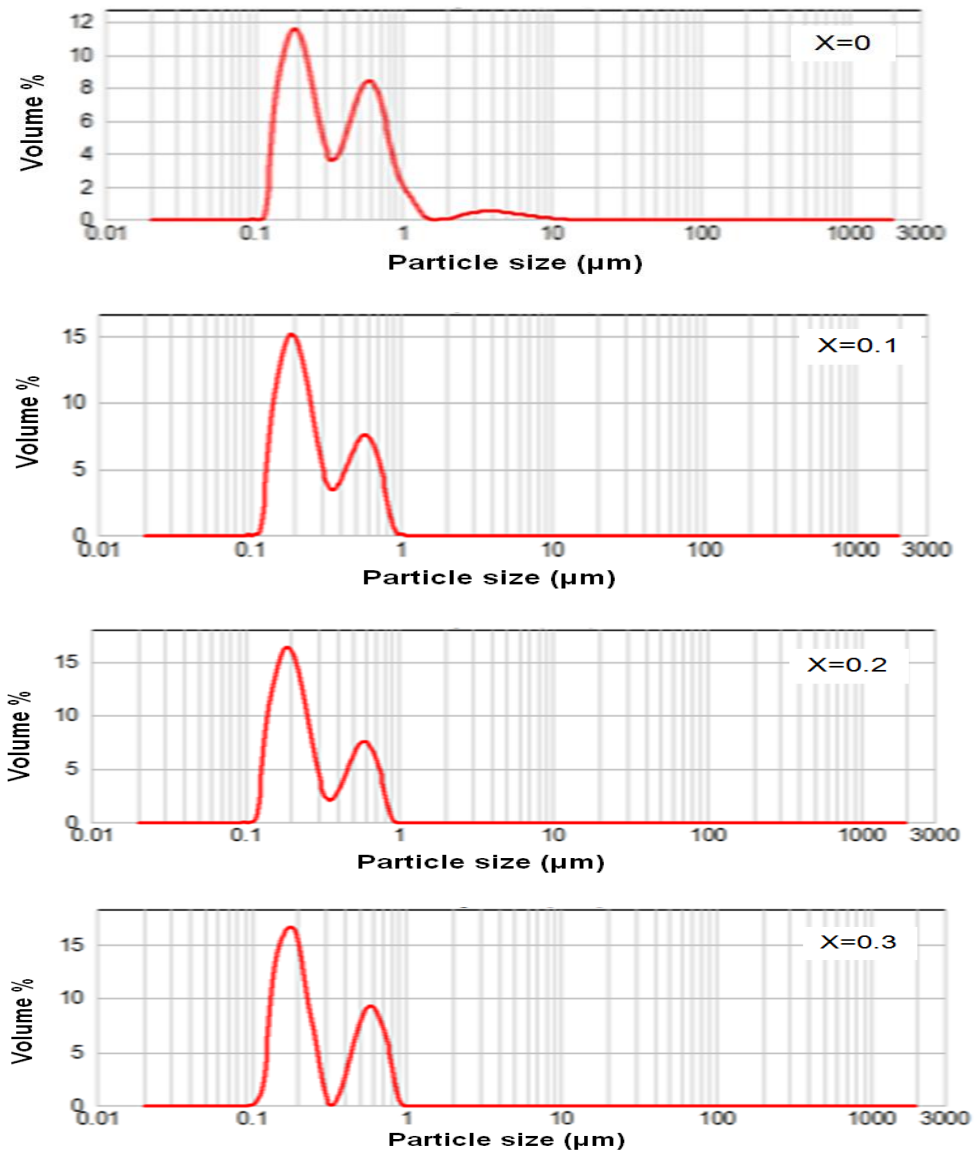


Figure 6. Particle size distribution of samples SrCo<sub>1-x</sub>Cu<sub>x</sub>O<sub>3-δ</sub> with x=0, 0.1, 0.2, 0.3.

Consequently, the cell volume gradually when the substitution  $x$  increases from 0 to 0.3 (Figure 4) are due to the significant decrease in the parameters  $a$  and  $c$ .

### 3.3. Crystallite size and distribution by volume particle size of $\text{SrCo}_{1-x}\text{Cu}_x\text{O}_{3-\delta}$ powder

The average crystallite size ( $D$ ) was evaluated from the broadening of the XRD line width by applying the Scherer's formula (Figure 5). It is observed that crystallite size decreases with increasing copper content. This is probably due to the incorporation of  $\text{Cu}^{2+}$  into the  $\text{SrCoO}_{3-\delta}$  lattice which leads to the crystallite decrease.

Figure 6 shows that the particle size distribution in volume of  $\text{SrCo}_{1-x}\text{Cu}_x\text{O}_{3-\delta}$  samples with  $x=0, 0.1, 0.2$  and  $0.3$ , the average diameters in volume  $D_v(0.5) = 0.307; 0.236; 0.225; 0.213 \mu\text{m}$  respectively. This result also indicates that the powders are highly agglomerated. This is could be due to the agglomeration of ultra-fine powders, present in the suspension.

### 4. CONCLUSIONS

Four powders with nominal composition  $\text{SrCo}_{1-x}\text{Cu}_x\text{O}_{3-\delta}$ , ( $x = 0, 0.1, 0.2, 0.3$ ) have been synthesized by citrate sol-gel method. XRD patterns indicate that a stable perovskite phase with rhombohedral system has been obtained for all the compositions with no detectable secondary phase as confirmed by XRD and FT-IR. The crystallite size decreases with increasing the copper amount. The grain size of oxides as determined from laser diffraction is between  $0.213$

and  $0.307 \mu\text{m}$ . This result reveals that agglomerates are present in the suspension.

### REFERENCES

- [1] Grimaud, A., et al. *Nature Communications* **4**, 2439-2441(2013).
- [2] Jung J I, Jeong H Y, Kim M G, et al. *Advanced Materials* **27**,266-271(2015).
- [3] Lin Y, Ran R, Chen D, et al. *Journal of Power Sources* **195** , 4700-4703(2010).
- [4] Ludwig J. *Journal of Power Sources* **155**, 23-32 (2006).
- [5] Du Z, Yang, Peng, Wang, Long, et al. *Journal of Power Sources* **265** , 91- 96 (2014).
- [6] Shimizu, Y. Matsuda, H. Miura, N. Yamazoe. *Chem. Lett.* **21**, 1033–1036 (1992).
- [7] Duan, Y. Sun, S. Xi, S. Ren, X. Zhou, Y. Zhang, G. Yang, H. Du, Y. Xu, Z. *J. Chem. Mater.* **29**, 10534–10541(2017).
- [8] S.P. Jiang. *Journal of Materials Science* **43** (21), 6799–6833 (2008).
- [9] Xin S, Dong D, Parkinson G, et al. *Journal of Membrane Science* **454** ,444-450 (2014).
- [10] Shao Z.P., Haile S.M. *Nature* **431**, 170–173 (2004).
- [11] J. Richter, P. Holtappels, T. Graule, T. Nakamura and L. J. Gauckler. *Monatshefte für Chemie-Chemical Monthly.* **140**, 985-999 (2009).
- [12] A. F. Sammells, R. L. Cook, J. H. White, J. J. Osborne and R. C. MacDuff, *Solid State Ionics* **52**, 111-123 (1992).
- [13] D. Chen, C. Chen, Z. Zhang, Z. M. Baiyee, F. Ciucci and Z. Shao, *ACS Appl.Mater.Interfaces* **7**, 8562-8571 (2015).
- [14] C. De la Calle, A. Aguadero, J. Alonso and M. Fernández-Díaz, *Solid State Sci.* **10**, 1924-1935 (2008).
- [15] Hongtao Cui, Marcos Zayat, David Levy. *Journal of Non-Crystalline Solids* **352**, 3035–3040 (2006).
- [16] R.D. Shannon. Revised effective ionic radii and systematic studies of interatomic distances in halides and chalcogenides, *Acta Cryst.* **A32** 751-767(1976).
- [17] Makhloufi S. and Omari M. *J. Inorg. Organomet. Polym.* **26**, 32, (2016).